Synthesis and evaluation of a radioiodinated tracer with specificity for PARP-1 in vivo.

Filip Zmuda,[†,‡] *Gaurav Malviya,*[¥] *Adele Blair,*[†] *Marie Boyd,*[±] *Anthony J. Chalmers,*[‡] *Andrew Sutherland,*[†] and *Sally L. Pimlott**[#]

[†]WestCHEM, School of Chemistry, The Joseph Black Building, University of Glasgow, Glasgow G12 8QQ, UK.

[‡]Wolfson Whol Cancer Research Centre, Institute of Cancer Sciences, University of Glasgow, Glasgow G61 1QH, UK.

[¥]Nuclear Imaging, Cancer Research UK Beatson Institute, Glasgow G61 1BD, UK.

[±]Strathclyde Institute of Pharmacy and Biomedical Sciences, John Arbuthnott Building, University of Strathclyde, Glasgow, G4 0RE, UK.

[#]West of Scotland PET Centre, Greater Glasgow and Clyde NHS Trust, Glasgow G12 0YN, UK.

ABSTRACT. Interest in nuclear imaging of poly(ADP-ribose) polymerase-1 (PARP-1) has grown in recent years due to the ability of PARP-1 to act as a biomarker for glioblastoma and increased clinical use of PARP-1 inhibitors. This study reports the identification of a lead iodinated analog **5** of the clinical PARP-1 inhibitor olaparib as a potential single-photon emission computed tomography (SPECT) imaging agent. Compound **5** was shown to be a potent PARP-1 inhibitor in cell-free and cellular assays, and it exhibited mouse plasma stability but approximately 3-fold greater intrinsic clearance when compared to olaparib. An ^{123}I-labeled version of **5** was generated using solid state halogen exchange methodology. *Ex vivo* biodistribution studies of [^{123}I]-**5** in mice bearing subcutaneous glioblastoma xenografts revealed that the tracer had the ability to be retained in tumour tissue and bind to PARP-1 with specificity. These findings support further investigations of [^{123}I]-**5** as a non-invasive PARP-1 SPECT imaging agent.

INTRODUCTION.

Poly(ADP-ribose) polymerase 1 (PARP-1) is a nuclear protein responsible for various cellular processes including repair of single-stranded DNA breaks (SSB), cell division, gene transcription and apoptosis regulation.[1] The role of PARP-1 in DNA repair has made it a highly pursued therapeutic target resulting in the development of numerous PARP-1 inhibitors (PARPi) with cancer treatment in mind. Initial therapeutic strategies involved targeting cancers that are deficient in the BRCA-1 and BRCA-2 genes that encode proteins with roles in homologus recombination repair of double-stranded DNA breaks (DSB). The combination of PARPi induced deficiency of SSB repair and impaired DSB repair generates synthetic lethality in BRCA mutated cancer cells while healthy tissues with intact BRCA function were not affected.[2–3] Compound **1** (olaparib) (Figure 1) is a PARPi that has recently been licenced in the EU and US as monotherapy for advanced BRCA deficient ovarian cancer[4] making it the most clinically advanced compound in its class.

In addition to synthetic lethality, PARPi are also being clinically assessed as adjuncts to chemotherapy where inhibition of PARP-1 mediated DNA repair sensitizes cancer cells to cytotoxic agents. However, a number of early phase clinical trials have reported severe bone marrow toxicity with such therapeutic combinations[5–10] which could in part be attributed to sub-optimal dosing schedules.[8] Non-invasive *in vivo* imaging of PARP-1 using a radiolabeled PARPi and techniques such as Positron Emission Tomography (PET) or Single-Photon Emission Tomography (SPECT) could be used to assess the duration of PARP-1 inhibition in different tissues. This could subsequently guide dosing decisions for PARPi when given in combination with chemotherapy such that tumour cytotoxicity is maximized and bone marrow toxicity is minimized. Furthermore, molecular imaging of PARP-1 could be utilized by clinicians to

evaluate the levels of PARP-1, as well as the extent of PARP-1 inhibition, in tumors in order to eliminate patients that are unlikely to respond to PARP-1 inhibitor therapy. There is a clinical need for this kind of information as the use of PARPi as mono- and combination therapy is becoming more prominent. PARP-1 could also be used as a molecular imaging biomarker for visualization of glioblastoma (GBM) which is known to overexpress PARP-1 in contrast to surrounding brain tissue where PARP-1 levels are low.[11] This type of imaging could be exploited for pre-surgical planning of GBM treatment, since conventional magnetic resonance imaging techniques lack the necessary sensitivity and specificity to delineate tumor from non-tumor tissue.[12]

With applications such as these it is not surprising that molecular imaging tracers for PARP-1 are being developed. At the time of writing all current PARP-1 tracers are being developed for the PET imaging modality (compounds **2**–**4**, Figure 2)[13–15] and to the best of our knowledge there are no SPECT radiotracers in development. In recent years PET imaging has gained a lot of traction in clinical environments due to shorter scan durations, superior sensitivity and spatial resolution, and availability of combined modality imaging (e.g. PET/CT) when compared to SPECT.[16–17] However, hybrid SPECT/CT devices are now in general clinical use and new technology is emerging which has the capability to significantly improve spatial resolution.[17] An important advantage of SPECT over PET is the ability to perform simultaneous dual-tracer imaging[16] which could be utilized as a powerful tool when comparing existing to novel radiotracers. Furthermore, the established nature of this molecular imaging modality means that clinical SPECT scanners are currently more widely available than PET scanners.[18] For these reasons, the SPECT modality is likely to remain a key component of nuclear medicine

for many years to come and radiotracer development for SPECT imaging should not be neglected.

Therefore, we proposed to use the structure of the clinical PARPi **1** in the pursuit of a novel PARP-1 SPECT imaging radiotracer. It has been shown that binding of **1** to the PARP-1 active site can tolerate structural modifications in the cyclopropane bearing region.[19–20] Utilizing this, we report the synthesis of a small library of novel cold (non-radioactive) iodinated analogs of **1** with structural variance in the cyclopropane region, which were designed to represent potential PARP-1 SPECT imaging agents. An iodinated compound is extremely versatile, having the potential to incorporate different iodine radionuclides, such as ^{123}I for SPECT imaging, ^{124}I for PET imaging and ^{131}I for radiotherapeutic application. We describe the physiochemical parameters and activity against PARP-1 of these compounds followed by the assessment of plasma and metabolic stability of the lead analog **5**. The radioiodination methodology and subsequent *ex vivo* biodistribution of the potential PARP-1 SPECT tracer [^{123}I]-**5** in mice bearing subcutaneous glioblastoma xenografts are also described.

RESULTS AND DISCUSSION.

Chemistry. The penultimate compound **6** (Table 1) which was used to access **1** and its analogs was synthesized using a slightly modified route to that described previously by Menear *et al*[20] (see supplementary information for details). An amide coupling reaction between **6** and the commercially available cyclopropane carboxylic acid formed **1**. Iodinated analogs (**5** and **7**–**12**) of **1** were accessed by either amide or N-sulfonyl coupling of the penultimate compound **6** with the corresponding commercially available carboxylic acid or sulfonyl chloride compounds

respectively as shown in Table 1. This approach allowed rapid access to a small library of cold iodinated compounds representing potential PARP-1 SPECT imaging agents.

In vitro characterization. Compounds **5** and **7**–**12** were screened *in vitro* for their ability to inhibit PARP-1 in a cell-free system and for their lipophilicity (log P_{oct}) and percentage plasma protein binding (%PPB) parameters using high performance liquid chromatography. The results of this screen are outlined in Table 1. The iodinated compounds exhibited low nanomolar cell-free PARP-1 IC_{50} values confirming that structural variance in the cyclopropane region of **1** had only a minor influence on PARP-1 inhibition potency.[19–20] The analogs also showed greater log P_{oct} ($\geq$ 2.95) and %PPB ($\geq$ 96.1%) values when compared to **1** (log P_{oct} = 1.95, %PPB = 75.9%). The increase in both parameters can be partly attributed to the presence of the lipophilic iodine-bearing benzyl moieties as plasma protein binding interactions are hydrophobic in nature.[21] Despite the increase in lipophilic properties, the log P_{oct} values of compounds **5**, **7** and **9** were within the optimal range (log P_{oct} = 1.5–3.0) for passage across cellular membranes[22] which is important as PARP-1 is localized within cellular nuclei. Under normal circumstances large macromolecules such as plasma proteins are unable to penetrate into the brain due to the presence of the Blood-Brain Barrier (BBB). However, numerous pathologies of the brain including tumors are associated with disruptions of the BBB.[23] This, coupled with the fact that tumors are known to actively take up plasma proteins[24] has made it possible to target gliomas with fluorescent- and radiolabelled human plasma protein conjugates for fluorescent[25] and SPECT[26] imaging respectively. It is therefore proposed that the extensive plasma protein binding of analogs **5** and **7**–**12** could provide an additional means of passive targeting for the molecular imaging of tumors including GBM.

Compound **5** was selected as the lead candidate for further assessment due to its cell-free PARP-1 inhibitory potency (cell-free IC_{50} 3.3 nM), optimal lipophilic properties (log P_{oct} = 3.0) and the radiochemically accessible *para* position of the iodine atom. Cellular IC_{50} values in primary G7 and established T98G human glioblastoma cell lines were ascertained in order to confirm the PARP-1 inhibitory potency of **5** in cellular systems (Table 2). A slight reduction in cellular compared with cell-free PARP-1 inhibitory potency was observed (3.3 nM vs. 7.0 nM in G7 and 7.4 nM in T98G cells) which can be explained by the fact that in the former case activity requires cellular penetration and retention, unlike the cell-free assay. Despite this slight reduction in potency, **5** remained an effective PARP-1 inhibitor in living cells, confirming its ability to enter tumour cells *in vitro*.

The stability of **5** was investigated in presence of mouse plasma proteins and human liver microsomes. Compound **5** was shown to be stable in mouse plasma over a 20 h period with no noticeable degradation taking place (Table 2). The intrinsic clearance (Cl_{int}), an *in vitro* parameter of metabolic stability,[27] of **5** was markedly greater than that of **1** (Cl_{int} = 85 ± 4 vs. 29 ± 4 μL/min/mg) suggesting more rapid *in vivo* metabolism of the analog (Table 2). The terminal aromatic-halide moiety of **5** is likely to undergo liver enzyme oxidation and dehalogenation, which might explain the observed reduction in metabolic stability.[28] This is in contrast to the metabolically stable cyclopropane moiety of **1**.[29] Furthermore, since a positive correlation exists between lipophilicity and rate of metabolism, the increase in log P_{oct} of **5** may have also been a contributing factor to the increase in Cl_{int}.[21]

Radiochemistry. Following *in vitro* characterization of **5** focus was shifted towards generating a radioiodinated version of this compound. Initial efforts to obtain the stannyl

precursor for the destannylation radioiodindation of **5** were unsuccessful. Therefore, solid state aromatic halogen exchange radioiodination methodology was investigated based on our past successful experiences with this technique.[30] The bromine analog **13**, accessed by amide coupling of the penultimate compound **6** with commercially available 4-bromobenzoic acid, was used as the radiolabelling precursor (Table 3). For practical reasons, optimization of the radiolabelling reaction was performed using the long lived ^{125}I-radionuclide (half-life of ^{125} I = 60.1 days vs. ^{123}I = 13.2 hours). The reaction conditions described by Gildersleeve *et al*[31] (entry 1) were used as a starting point which allowed for an ^{125}I incorporation yield of 38% (n = 1). By increasing the temperature and the reaction time (entry 3) an improved yield of 90% (n = 1) was achieved. The drop in radioiodide incorporation in the absence of air (entry 4) was not unexpected as a mildly oxidizing environment is necessary for efficient solid state halogen exchange to take place.[32] The conditions described in entry 3 were identified as optimal and were used for ^{123}I-radiolabelling (Scheme 1) giving access to the potential SPECT imaging agent [^{123}I]-**5** in a non-decay corrected end of synthesis yield of 36.5 ± 7.2% (n = 6) and a specific activity of >19.0 ± 10.3 Ci/μmol (n = 4).

Ex vivo **biodistribution.** In order to assess the behaviour of [^{123}I]-**5** *in vivo* the biodistribution of the radioligand was investigated in female nude mice bearing subcutaneous human glioblastoma xenografts by gamma-counting of harvested animal materials and tissues 30, 60 and 120 min after intravenous injection of the radiotracer. The large amounts of radioactivity present in the liver and small bowel matter 30 min after injection and the subsequent gradual increase of radioactivity in solid feces were indicative of rapid hepatobilliary clearance of [^{123}I]-**5** (Figure 3). This type of clearance is in line with previous observations made for **1**.[33] Despite rapid *in vivo* clearance, a significant increase in the mean ratio of percentage

injected dose per gram (%ID/g) of tumor to muscle was observed between the 30 and 120 min timepoints (2.15 ± 0.47 to 5.61 ± 1.99) providing clear evidence of radioligand retention within the tumor (unpaired t test: P = 0.036). Immunohistochemical staining of tumor tissue showed high levels of proliferative cells and PARP-1 expression. This is in contract to muscle tissue where the proliferative marker (Ki67) and PARP-1 were not detectable (Figure 4). The negligible uptake of [^{123}I]-**5** in the brain can be explained by low PARP-1 expression in healthy brain tissue and,[11] with the exception of log P_{oct}, physiochemical parameters that fall outside of those optimal for BBB penetration (optimal parameters: log P_{oct} = 2–3[21], MW <450[34], %PPB <95%[35]). Chalmers *et al* reported similar findings which showed that after a single dose of [^{14}C]-**1** there was no detectable radioactivity in the central nervous system of subcutaneous colorectal cancer xenograft bearing rats. However, the authors were able to show therapeutic levels of **1** in resected GBM specimens from patients who received oral doses of the drug.[36] Therefore, we hypothesize that BBB disruptions associated with GBM[23] will allow for uptake of [^{123}I]-**5** in brain tumor tissue. It is important to confirm that the uptake of [^{123}I]-**5** in tumor was due to the specific binding of the radioligand to PARP-1. This was achieved by blocking PARP-1 binding sites through the pre-treatment of subcutaneous tumor bearing mice with 50 mg/kg unlabelled compound **1** intraperitonally 20 min prior to radiotracer administration (Figure 5). Pre-blockade with **1** resulted in a significant decrease in the ratio of %ID/g of tumour to muscle from 2.59 ± 0.06 to 1.30 ± 0.13 when compared to the vehicle treated cohort (unpaired t test: P = 0.001). This observation confirms the specificity of [^{123}I]-**5** for PARP-1 *in vivo*.

CONCLUSIONS.

In an effort to develop a novel PARP-1 SPECT radiotracer we have generated a small library of cold iodinated analogs based on the clinical PARP-1 inhibitor **1,** designed to represent potential SPECT imaging agents. *In vitro* characterization of these compounds led to the identification of **5** as a lead candidate due to its low nanomolar PARP-1 cell-free IC_{50}. The compound was revealed to be a potent PARP-1 inhibitor in two human glioblastoma cell lines and it was stable in mouse plasma, but exhibited approximately 3-fold greater *in vitro* clearance when compared to **1**. Radioiodination methodology was developed and the *in vivo* behaviour of [^{123}I]-**5** was assessed in mice bearing a subcutaneous human glioblastoma xenograft model. *Ex vivo* biodistribution revealed rapid hepatobiliary clearance of [^{123}I]-**5**. Despite that, the radioligand exhibited tumor tissue retention and specific binding to PARP-1 *in vivo*. Collectively, these findings support further *in vivo* evaluation of [^{123}I]-**5** as a PARP-1 SPECT imaging agent.

EXPERIMENTAL SECTION.

All reagents and starting materials were obtained from commercial sources and used as received. All dry solvents were purified using a solvent purification system. All reactions were performed under an atmosphere of argon unless otherwise mentioned. Flash column chromatography was performed using Fisher matrix silica gel 60 (35–70 μm). Macherey-Nagel aluminium-backed plates pre-coated with silica gel $60F_{254}$ were used for thin layer chromatography and were visualized with a UV lamp or by staining with potassium permanganate. ^{1}H NMR spectra were recorded on a Bruker DPX 400 spectrometer or a Bruker 500 spectrometer and data are reported as follows: chemical shift in ppm relative to Me_4Si or the solvent ($CDCl_3$, δ 7.26 ppm, CD_3OD, δ 3.31 ppm or DMSO-δ_6, δ 2.50 ppm) as the internal

standard, multiplicity (s = singlet, d = doublet, t = triplet, q = quartet, m = multiplet or overlap of nonequivalent resonances, integration). ^{13}C NMR spectra were recorded on a Bruker DPX NMR spectrometer at either 101 or 126 MHz and data are reported as follows: chemical shift in ppm relative to Me_4Si or the solvent as internal standard ($CDCl_3$, δ 77.2 ppm, CD_3OD, δ 49.0 ppm or DMSO-δ_6, δ 39.5 ppm), multiplicity with respect to proton (deduced from DEPT experiments, C, CH, CH_2 or CH_3). Infrared spectra were recorded using a Shimadzu IRPrestige-21 spectrometer; wavenumbers are indicated in cm^{-1}. Mass spectra were recorded using electron impact, chemical ionization or electrospray techniques. HRMS spectra were recorded using a JEOL JMS-700 spectrometer. Melting points are uncorrected. All compounds used for biological testing exhibited >95% purity as per HPLC. Mice used for *in vivo* studies were housed in individually ventilated cages and had access to sterilized food and water *ad libitum*. All animal experiments were carried out in compliance with UK Home Office regulations.

4-[3'-(4''-Cyclopropanecarbonylpiperazine-1''-carbonyl)-4'-fluorobenzyl]-2*H*-phthalazin-1-one (1).[20] To a solution of cyclopropanoic acid (11.0 μL, 0.137 mmol) in DMF (2 mL) was added Et_3N (29.0 μL, 0.218 mmol), followed by HBTU (57.0 mg, 0.150 mmol), and the mixture was stirred at room temperature for 1 h. Following this **6** (50.0 mg, 0.137 mmol) was then added and the mixture was stirred for a further 72 h. The crude product was extracted into $CHCl_3$ (3 × 10 mL) and the organic layer was washed with water (6 × 20 mL), dried with $MgSO_4$, filtered and concentrated *in vacuo* to give a yellow solid. Purification by flash column chromatography (MeOH/CH_2Cl_2, 4:96) gave **1** (30 mg, 51%) as a white foam. ^{1}H NMR spectra showed a 3:2 mixture of rotamers. Only data for the major rotamer were recorded. ^{1}H NMR (400 MHz, $CDCl_3$) δ 0.67–0.86 (m, 2H), 0.97–1.03 (m, 2H), 1.75 (br s, 1H), 3.20–3.43 (m, 2H), 3.51–3.93

(m, 6H), 4.29 (s, 2H), 7.04 (t, *J* 8.9 Hz, 1H), 7.29–7.41 (m, 2H), 7.67–7.82 (m, 3H), 8.43–8.51 (m, 1H), 11.12 (br s, 1H); ^{13}C NMR (101 MHz, $CDCl_3$) δ 7.8 (2 × CH_2), 11.2 (CH), 37.8 (CH_2), 41.8 (CH_2), 42.4 (CH_2), 45.3 (CH_2), 47.0 (CH_2), 116.3 (CH, d, $J_{C\text{-}C\text{-}F}$ 22.3 Hz), 123.9 (C, d, $J_{C\text{-}C\text{-}F}$ 18.3 Hz), 125.1 (CH), 127.3 (CH), 128.5 (C), 129.4 (CH), 129.7 (C), 131.7 (CH), 131.8 (CH, d, $J_{C\text{-}C\text{-}C\text{-}F}$ 8.1 Hz), 133.8 (CH), 134.5 (C, d, $J_{C\text{-}C\text{-}C\text{-}C\text{-}F}$ 3.4 Hz), 145.6 (C), 157.2 (C, d, $J_{C\text{-}F}$ 247.4 Hz), 160.7 (C), 165.3 (C), 172.4 (C); HRMS (ESI) calcd for $C_{24}H_{23}FN_4NaO_3$ (MNa^+), 457.1646, found 457.1636.

4-[3'-[4''-(4'''-Iodobenzoyl)piperazine-1''-carbonyl]-4'-fluorobenzyl]-2*H*-phthalazin-1-one (5). To a solution of 4-iodobenzoic acid (42.0 mg, 0.170 mmol) in DMF (7 mL) was added Et_3N (37.0 μL, 0.272 mmol), followed by HBTU (71.0 mg, 0.187 mmol) and the mixture was stirred at room temperature for 2 h. Following this **6** (60.0 mg, 0.170 mmol) was added and the mixture was stirred for a further 48 h. Water (14 mL) was then added, followed by 1 h of stirring after which the mixture was cooled to 0 °C. The resulting precipitate was collected by vacuum filtration and washed with Et_2O (4 × 10 mL) and hexane (4 × 10 mL). Purification by flash column chromatography (MeOH/CH_2Cl_2, 4:96) gave **5** (34.8 mg, 34%) as a white foam. IR (neat) 3198, 3003, 2899, 1628, 1587, 1427, 1001, 747 cm^{-1}; ^{1}H NMR (400 MHz, $CDCl_3$) δ 3.14–4.02 (m, 8H), 4.29 (s, 2H), 7.03 (t, *J* 7.8 Hz, 1H), 7.14 (d, *J* 8.0 Hz, 2H), 7.29–7.37 (m, 2H), 7.67–7.84 (m, 5H), 8.42–8.51 (m, 1H), 10.96 (s, 1H); ^{13}C NMR (101 MHz, $CDCl_3$) δ 37.8 (CH_2), 42.2 (2 × CH_2), 47.3 (2 × CH_2), 96.6 (C), 116.3 (CH, d, $J_{C\text{-}C\text{-}F}$ 21.7 Hz), 123.6 (C, d, $J_{C\text{-}C\text{-}F}$ 17.7 Hz), 125.1 (CH), 127.3 (CH), 128.4 (C), 128.9 (2 × CH), 129.4 (CH, d, $J_{C\text{-}C\text{-}C\text{-}F}$ 3.6 Hz), 129.6 (C), 131.8 (CH), 131.9 (CH, d, $J_{C\text{-}C\text{-}F}$ 8.0 Hz), 133.8 (CH), 134.5 (C), 134.6 (C, d, $J_{C\text{-}C\text{-}C\text{-}C\text{-}F}$ 3.7 Hz), 138.0 (2 × CH), 145.6 (C), 157.1 (C, d, $J_{C\text{-}F}$ 247.1 Hz), 160.7 (C), 165.3 (C), 169.8 (C); HRMS (ESI) calcd for $C_{27}H_{22}FIN_4NaO_3$ (MNa^+), 619.0613, found 619.0597.

4-[3'-[4''-(3'''-Iodobenzoyl)piperazine-1''-carbonyl]-4'-fluorobenzyl]-2*H*-phthalazin-1-one (7). The reaction was carried out as described for **5** using a solution of 3-iodobenzoic acid (34.0 mg, 0.137 mmol) in DMF (3 mL), Et_3N (29.0 μL, 0.218 mmol), HBTU (57.0 mg, 0.151 mmol) and **6** (50.0 mg, 0.137 mmol). Purification by flash column chromatography ($MeOH/CH_2Cl_2$, 4:96) gave **7** (36.4 mg, 45%) as a white foam. IR (neat) 3190, 3053, 2862, 1628, 1559, 1427, 1252, 1005, 791, 729 cm^{-1}; ^1H NMR (400 MHz, $CDCl_3$) δ 3.16–4.01 (m, 8H), 4.29 (s, 2H), 7.03 (br s, 1H), 7.15 (br s, 1H), 7.27–7.39 (m, 3H), 7.67–7.82 (m, 5H), 8.42–8.49 (m, 1H), 10.70 (s, 1H); ^{13}C NMR (101 MHz, $CDCl_3$) δ 37.8 (CH_2), 42.2 (2 × CH_2), 47.4 (2 × CH_2), 94.5 (C), 116.3 (CH, d, $J_{C\text{-}C\text{-}F}$ 21.7 Hz), 123.6 (C, d, $J_{C\text{-}C\text{-}F}$ 17.7 Hz), 125.1 (CH), 126.2 (CH), 127.3 (CH), 128.4 (C), 129.4 (CH, d, $J_{C\text{-}C\text{-}C\text{-}F}$ 3.6 Hz), 129.6 (C), 130.4 (CH), 131.8 (CH), 131.9 (CH, d, $J_{C\text{-}C\text{-}C\text{-}F}$ 8.0 Hz), 133.8 (CH), 134.6 (C, d, $J_{C\text{-}C\text{-}C\text{-}C\text{-}F}$ 3.9 Hz), 136.0 (CH), 137.1 (C), 139.2 (CH), 145.6 (C), 157.1 (C, d, $J_{C\text{-}F}$ 247.1 Hz), 160.8 (C), 165.3 (C), 168.8 (C); HRMS (ESI) calcd for $C_{27}H_{22}FIN_4NaO_3$ (MNa^+), 619.0613, found 619.0605.

4-[3'-[4''-(3'''-Iodo-4'''-methylbenzoyl)piperazine-1''-carbonyl]-4'-fluorobenzyl]-2*H*-phthalazin-1-one (8). To a solution of 3-iodo-4-methylbenzoic acid (36.0 mg, 0.137 mmol) in DMF (3 mL) was added Et_3N (29.0 μL, 0.218 mmol), followed by HBTU (57.0 mg, 0.151 mmol) and the mixture was stirred at room temperature for 1 h. Following this, **6** (50.0 mg, 0.137 mmol) was then added and the mixture was stirred for a further 22 h at 40 °C. The mixture was cooled to room temperature and water (6 mL) was added, followed by 1 h of stirring after which the mixture was cooled to 0 °C. The resulting precipitate was collected by vacuum filtration and dissolved in $CHCl_3$ (10 mL). The organic layer was washed with water (3 × 20 mL) and concentrated *in vacuo*. Purification by flash column chromatography ($MeOH/CH_2Cl_2$, 3:97) gave **8** (40.0 mg, 48%) as a white foam. IR (neat) 3203, 3011, 2893, 1629, 1425, 1252, 1006, 746 cm^{-}

[1]; ^{1}H NMR (400 MHz, $CDCl_3$) δ 2.44 (s, 3H), 3.13–4.05 (m, 8H), 4.27 (s, 2H), 7.03 (t, *J* 8.4 Hz, 1H), 7.23–7.37 (m, 4H), 7.67–7.80 (m, 3H), 7.85 (s, 1H), 8.43–8.49 (m, 1H), 10.85 (s, 1H); ^{13}C NMR (101 MHz, $CDCl_3$) δ 28.2 (CH_3), 37.8 (CH_2), 42.3 (2 × CH_2), 47.1 (2 × CH_2), 101.1 (C), 116.3 (CH, d, $J_{C\text{-}C\text{-}F}$ 22.0 Hz), 123.7 (C, d, $J_{C\text{-}C\text{-}F}$ 17.6 Hz), 125.1 (CH), 127.0 (CH), 127.3 (CH), 128.4 (C), 129.4 (CH, d, $J_{C\text{-}C\text{-}C\text{-}F}$ 3.2 Hz), 129.6 (C), 129.8 (CH), 131.8 (CH), 131.9 (CH, d, $J_{C\text{-}C\text{-}C\text{-}F}$ 7.8 Hz), 133.8 (CH), 134.2 (C), 134.6 (C, d, $J_{C\text{-}C\text{-}C\text{-}C\text{-}F}$ 3.8 Hz), 137.6 (CH), 143.9 (C), 145.6 (C), 157.1 (C, d, $J_{C\text{-}F}$ 249.9 Hz), 160.8 (C), 165.3 (C), 168.9 (C); HRMS (ESI) calcd for $C_{28}H_{24}FIN_4NaO_3$ (MNa^+), 633.0769, found 633.0759.

4-[3'-[4''-(3'''-Iodo-4'''-methoxybenzoyl)piperazine-1''-carbonyl]-4'-fluorobenzyl]-2*H*-phthalazin-1-one (9). The reaction was carried out as described for **5** using a solution of 3-iodo-4-methoxybenzoic acid (76.0 mg, 0.273 mmol) in DMF (5 mL), Et_3N (59.0 μL, 0.437 mmol), HBTU (114 mg, 0.300 mmol) and **6** (100 mg, 0.273 mmol). Purification by flash column chromatography (MeOH/CH_2Cl_2, 3:97) gave **9** (44.5 mg, 26%) as a white foam. IR (neat) 3192, 3009, 2897, 1628, 1593, 1425, 1256, 1005, 747 cm^{-1}; ^{1}H NMR (400 MHz, $CDCl_3$) δ 3.34 (br s, 2H), 3.45–3.85 (m, 6H), 3.90 (s, 3H), 4.29 (s, 2H), 6.82 (d, *J* 8.3 Hz, 1H), 7.03 (t, *J* 8.7 Hz, 1H), 7.29–7.36 (m, 2H), 7.40 (dd, *J* 8.3, 2.0 Hz, 1H), 7.68–7.81 (m, 3H), 7.85 (d, *J* 2.0 Hz, 1H), 8.43–8.50 (m, 1H), 10.82 (s, 1H); ^{13}C NMR (101 MHz, $CDCl_3$) δ 37.8 (CH_2), 42.3 (2 × CH_2), 47.2 (2 × CH_2), 56.7 (CH_3), 86.0 (C), 110.6 (CH), 116.3 (CH, d, $J_{C\text{-}C\text{-}F}$ 21.7 Hz), 123.6 (C, d, $J_{C\text{-}C\text{-}F}$ 17.7 Hz), 125.1 (CH), 127.4 (CH), 128.5 (C), 129.1 (C), 129.3 (CH), 129.4 (CH, d, $J_{C\text{-}C\text{-}C\text{-}F}$ 3.6 Hz), 129.7 (C), 131.8 (CH), 131.9 (CH, d, $J_{C\text{-}C\text{-}C\text{-}F}$ 8.0 Hz), 133.8 (CH), 134.6 (C, d, $J_{C\text{-}C\text{-}C\text{-}C\text{-}F}$ 3.9 Hz), 138.8 (CH), 145.6 (C), 157.1 (C, d, $J_{C\text{-}F}$ 247.1 Hz), 159.7 (C), 160.6 (C), 165.3 (C), 169.0 (C); HRMS (ESI) calcd for $C_{28}H_{24}FIN_4NaO_4$ (MNa^+), 649.0718, found 649.0713.

4-[3'-[4''-[2'''-(3''''-Iodophenyl)acetyl]piperazine-1''-carbonyl]-4'-fluorobenzyl]-2*H*-phthalazin-1-one (10). The reaction was carried out as described for **5** using a solution of 3-iodophenylacetic acid (72.0 mg, 0.273 mmol) in DMF (5 mL), triethylamine (59.0 μL, 0.437 mmol), HBTU (114 mg, 0.300 mmol) and **6** (100 mg, 0.273 mmol). Purification by flash column chromatography ($MeOH/CH_2Cl_2$, 3:97) gave **10** (67.0 mg, 40%) as a white foam. NMR spectra showed a 55:45 mixture of rotamers. Only data for the major rotamer were recorded. IR (neat) 3190, 3005, 2899, 1632, 1589, 1433, 1223, 1013, 748 cm^{-1}; ^1H NMR (400 MHz, $CDCl_3$) δ 3.27 (br s, 2H), 3.39 (t, J 4.6 Hz, 2H), 3.50–3.90 (m, 6H), 4.28 (s, 2H), 6.97–7.10 (m, 2H), 7.14–7.24 (m, 1H), 7.29–7.37 (m, 2H), 7.53–7.63 (m, 2H), 7.67–7.73 (m, 1H), 7.74–7.81 (m, 2H), 8.43–8.50 (m, 1H), 10.90 (br s, 1H); ^{13}C NMR (101 MHz, $CDCl_3$) δ 37.8 (CH_2), 40.3 (CH_2), 41.6 (CH_2), 42.1 (CH_2) 45.8 (CH_2), 46.8 (CH_2), 94.8 (C), 116.3 (CH, d, $J_{C\text{-}C\text{-}F}$ 21.7 Hz), 123.5 (C, d, $J_{C\text{-}C\text{-}F}$ 17.7 Hz), 125.0 (CH), 127.2 (CH), 128.1 (CH), 128.3 (C), 129.3 (CH, d, $J_{C\text{-}C\text{-}C\text{-}F}$ 3.3 Hz), 129.6 (C), 130.6 (CH), 131.7 (CH), 131.9 (CH, d, $J_{C\text{-}C\text{-}C\text{-}F}$ 7.9 Hz), 133.8 (CH), 134.6 (C, d, $J_{C\text{-}C\text{-}C\text{-}F}$ 3.2 Hz), 136.3 (CH), 136.9 (C), 137.7 (CH), 145.6 (C), 157.0 (C, d, $J_{C\text{-}F}$ 247.8 Hz), 161.0 (C), 165.3 (C), 169.1 (C); HRMS (ESI) calcd for $C_{28}H_{24}FIN_4NaO_3$ (MNa^+), 633.0769, found 633.0750.

4-[3'-[4''-[2'''-(4''''-Iodophenoxy)acetyl]piperazine-1''-carbonyl]-4'-fluorobenzyl]-2*H*-phthalazin-1-one (11). The reaction was carried out as described for **5** using a solution of 4-iodophenoxyacetic acid (76.0 mg, 0.273 mmol) in DMF (5 mL), Et_3N (59.0 μL, 0.437 mmol), HBTU (114 mg, 0.300 mmol) and **6** (100 mg, 0.273 mmol). Purification by flash column chromatography ($MeOH/CH_2Cl_2$, 4:96) gave **11** (55.0 mg, 32%) as a white foam. NMR spectra showed a 55:45 mixture of rotamers. Only data for the major rotamer were recorded. IR (neat) 3167, 3007, 2901, 1634, 1585, 1485, 1431, 1217, 1009, 745 cm^{-1}; ^1H NMR (400 MHz, $CDCl_3$) δ

3.22 (br s, 2H), 3.40–3.83 (m, 6H), 4.22 (s, 2H), 4.64 (s, 2H), 6.67 (d, *J* 6.7 Hz, 2H), 6.96 (t, *J* 8.6 Hz, 1H), 7.23–7.31 (m, 2H), 7.48 (t, *J* 9.2 Hz, 2H), 7.60–7.75 (m, 3H), 8.37–8.44 (m, 1H), 11.23 (s, 1H); ^{13}C NMR (101 MHz, $CDCl_3$) δ 37.7 (CH_2), 42.4 (2 × CH_2), 45.2 (CH_2), 46.8 (CH_2), 67.7 (CH_2), 84.4 (C), 116.3 (CH, d, $J_{C\text{-}C\text{-}F}$ 22.1 Hz), 117.0 (2 × CH), 123.5 (C, d, $J_{C\text{-}C\text{-}F}$ 17.6 Hz), 125.1 (CH), 127.3 (CH), 128.4 (C), 129.3 (CH, d, $J_{C\text{-}C\text{-}C\text{-}F}$ 3.4 Hz), 129.6 (C), 131.7 (CH), 131.9 (CH, d, $J_{C\text{-}C\text{-}C\text{-}F}$ 7.9 Hz), 133.8 (CH), 134.6 (C, d, $J_{C\text{-}C\text{-}C\text{-}C\text{-}F}$ 3.6 Hz), 138.6 (2 × CH), 145.6 (C), 157.0 (C, d, $J_{C\text{-}F}$ 247.4 Hz), 157.6 (C), 160.9 (C), 165.3 (C), 166.5 (C); HRMS (ESI) calcd for $C_{28}H_{24}FIN_4NaO_4$ (MNa^+), 649.0718, found 649.0714.

4-[3'-[4''-[4'''-Iodobenzenesulfonyl]piperazine-1''-carbonyl]-4'-fluorobenzyl]-2*H*-phthalazin-1-one (12). Et_3N (28.0 μL, 0.205 mmol) and 4-iodobenzenesulfonyl chloride (50.0 mg, 0.164 mmol) were added to a solution of **6** (50.0 mg, 0.137 mmol) in CH_2Cl_2 (3 mL). The mixture was stirred at room temperature for 6 h after which, water (3 mL) was added. The crude product was extracted into CH_2Cl_2 (3 × 10 mL), dried with Na_2SO_4, filtered and concentrated *in vacuo*. Purification by flash column chromatography (MeOH/CH_2Cl_2, 3:97) gave **12** (45.0 mg, 52%) as a white foam. IR (neat) 3185, 3006, 2895, 1637, 1568, 1438, 1349, 1164, 1005, 742 cm^{-1}; ^{1}H NMR (400 MHz, $CDCl_3$) δ 2.97 (t, *J* 4.8 Hz, 2H), 3.09 (br s, 2H), 3.39 (br s, 2H), 3.85 (br s, 2H), 4.27 (s, 2H), 7.00 (t, *J* 8.8 Hz, 1H), 7.24–7.34 (m, 2H), 7.40–7.46 (m, 2H), 7.66–7.72 (m, 1H), 7.73–7.80 (m, 2H), 7.88–7.93 (m, 2H), 8.44–8.51 (m, 1H), 11.31 (s, 1H); ^{13}C NMR (101 MHz, $CDCl_3$) δ 37.8 (CH_2), 41.5 (CH_2), 45.8 (CH_2), 46.2 (CH_2), 46.6 (CH_2), 101.0 (C), 116.3 (CH, d, $J_{C\text{-}C\text{-}F}$ 21.8), 123.4 (C, d, $J_{C\text{-}C\text{-}F}$ 17.9 Hz), 125.1 (CH), 127.3 (CH), 128.4 (C), 129.1 (2 × CH), 129.5 (CH, d, $J_{C\text{-}C\text{-}C\text{-}F}$ 3.5 Hz), 129.7 (C), 131.8 (CH), 132.0 (CH, d, $J_{C\text{-}C\text{-}C\text{-}F}$ 8.1 Hz), 133.8 (CH), 134.6 (C, d, $J_{C\text{-}C\text{-}C\text{-}C\text{-}F}$ 3.2 Hz), 135.4 (C), 138.7 (2 × CH), 145.6 (C), 156.9 (C, d, $J_{C\text{-}F}$

247.7 Hz), 160.8 (C), 165.0 (C); HRMS (ESI) calcd for $C_{26}H_{22}FIN_4NaO_4S$ (MNa^+), 655.0283, found 655.0274.

4-[3'-[4''-(4'''-Bromobenzoyl)piperazine-1''-carbonyl]-4'-fluorobenzyl]-2*H*-phthalazin-1-one (13). The reaction was carried out as described for **5** using a solution of 4-bromobenzoic acid (165 mg, 0.820 mmol) in DMF (10 mL), Et_3N (177 μL, 1.31 mmol), HBTU (341 mg, 0.900 mmol). Following the addition of **6** (300 mg, 0.820 mmol), the mixture was stirred at room temperature for 72 h, after which water (30 mL) was added and the solution was stirred for an additional 1 h. The mixture was cooled to 0 °C and the resulting precipitate was collected by vacuum filtration, washed with water (4 × 30 mL) and dried *in vacuo* to yield **13** (424 mg, 94%) as a yellow-white foam. IR (neat) 3233, 2934, 1668, 1622, 1593, 1460, 1433, 1269, 1221, 1003, 772 cm^{-1}; ^1H NMR (500 MHz, $CDCl_3$) δ 3.20–4.00 (m, 8H), 4.31 (s, 2H), 7.06 (br s, 1H), 7.27–7.39 (m, 4H), 7.52–7.63 (m, 2H), 7.70–7.75 (m, 1H), 7.75–7.78 (m, 2H), 8.46–8.53 (m, 1H), 10.99 (s, 1H); ^{13}C NMR (126 MHz, $CDCl_3$) δ 37.7 (CH_2), 42.2 (2 × CH_2), 47.0 (2 × CH_2), 116.2 (CH, d, $J_{C\text{-}C\text{-}F}$ 23.1 Hz), 123.5 (C, d, $J_{C\text{-}C\text{-}F}$ 17.6 Hz), 124.6 (C), 125.0 (CH), 127.2 (CH), 128.3 (C), 128.8 (2 × CH), 129.3 (CH, d, $J_{C\text{-}C\text{-}C\text{-}F}$ 3.5 Hz), 129.5 (C), 131.6 (CH), 131.8 (CH, d, $J_{C\text{-}C\text{-}C\text{-}F}$ 8.0 Hz), 132.0 (2 × CH), 133.7 (CH), 133.8 (C), 134.5 (C, d, $J_{C\text{-}C\text{-}C\text{-}C\text{-}F}$ 3.5 Hz), 145.5 (C), 156.9 (C, d, $J_{C\text{-}F}$ 248.3 Hz), 160.5 (C), 165.2 (C), 169.6 (C); HRMS (ESI) calcd for $C_{27}H_{22}{}^{79}BrFN_4NaO_3$ (MNa^+), 571.0752, found 571.0732.

HPLC Methodology. All physicochemical analyses were performed using a Dionex Ultimate 3000 series, and data acquisition and processing performed using the Chromeleon 6.8 Chromatography software. The HPLC system was set to 25 °C, and UV detection achieved using a diode array detector (190–800 nm).

Lipophilicity (log P_{oct}). Compounds **1**, **5** and **7**–**12** were dissolved in a 1:1 mixture of MeCN and 0.01 mM PBS to achieve a concentration of 0.5−1.5 mg/mL. The mean retention time of each compound was measured three times using a reverse phase Phenomenex Luna 5 μm C18 100Å (50 × 30 mm) column under the following mobile phase conditions: 0.0−10.5 min 100:0 to 10:90 A:B, 10.5−11.5 min 10:90 A:B, 11.5−12.5 minutes 10:90 to 100:0 A:B, 12.5−15.0 min 100:0 A:B where A = PBS and B = MeCN. The mobile phase flow rate was 1.0 mL/min. Three separate experiments were performed using PBS pH 4.0, pH 7.4, and pH 10.0. The necessary pH was achieved by addition of either HCl 0.1% or 0.05 M NH_4OH. A calibration regression model was generated by plotting the mean retention times (n = 3) against the known chromatographic hydrophobicity indices (CHIs) of the following standard compounds: theophylline (CHI = 15.76), phenyltetrazole (CHI = 20.18), benzimidazole (CHI = 30.71), colchicine (CHI = 41.37), acetophenone (CHI = 64.90), indole (CHI = 69.15), and butyrophenone (CHI = 88.49).[38] The CHI values of unknown compounds in the non-ionized state (CHIN) were obtained by fitting the mean retention times to the calibration regression model. The CHIN values were then converted to log P_{oct} values using the below equation:[39]

$$\text{Log } P_{oct} = 0.047\ \text{CHIN} + 0.036\ \text{HBC} - 1.10$$

where CHIN = the chromatographic hydrophobicity index of the non-ionized compound, and HBC = hydrogen-bond donor count. All calculations were performed and plots were generated using the Microsoft Excel 2010 software.

Percentage Plasma Protein Binding (%PPB). Compounds **1**, **5** and **7**–**12** were dissolved in a 1:3:3 mixture of MeCN, 0.01 mM PBS and IPA to achieve a concentration of 0.5–1.5 mg/mL. The mean retention time of each compound was measured three times using a ChromTech HSA

5 μm (50 × 30 mm) column under the following mobile phase conditions: 0.0–3.0 min 100:0 to 70:30 A:B, 3.0–10.5 min 70:30 A:B, 10.5–11.0 min 70:30 to 100:00 A:B, 11.0–15.0 min 100:0 A:B where A = PBS (pH 7.4) and B = IPA. The mobile phase flow rate was 1.8 mL/min. The chromatographic system was calibrated using the following standard compounds of known %PPB: nizatidine (%PPB = 35.0), bromazepam (%PPB = 60.0), carbamazepine (%PPB = 75.0), budesonide (%PPB = 88.0), nicardipine (%PPB = 95.0), warfarin (%PPB = 98.0), ketoprofen (%PPB = 98.7%), indomethacin (%PPB = 99.0), and diclofenac (%PPB = 99.8%).[39] The %PPB values of the standard compounds were converted to the linear free energy related log K values using the below equation:[40]

$$\text{Log k} = \log (\%\text{PPB} \div (101 - \%\text{PPB}))$$

A calibration regression model was generated by plotting the mean retention times (n = 3) of the standard compounds against their corresponding log K values. The log K values of unknown compounds were then obtained by fitting the mean retention times to the calibration regression model, which were then converted to %PPB values using the below equation:[40]

$$\%\text{PPB} = (101 \times 10^{\log k}) \div (1 + 10^{\log k})$$

All calculations were performed and plots were generated using the Microsoft Excel 2010 software.

Cell-free IC_{50}. A commercially available Trevigen® colorimetric PARP assay was used to determine the activity of PARP-1 in the presence of varying concentrations of compounds **1**, **5** and **7**–**12** in 96-well histone coated plates; the assays were performed as per the manufacturer protocol. Briefly, the compounds were dissolved in EtOH followed by serial dilution with the

supplied PARP buffer in order to attain the desired assay concentrations; the final concentration of EtOH in each case was <1%. To the histone-coated wells containing inhibitor was added 0.5 units of the supplied PARP enzyme diluted with PARP buffer. A positive control containing PARP enzyme in the absence of test compound and a negative control lacking PARP enzyme were also prepared. Following a 10 min incubation at room temperature a solution of PARP cocktail (containing biotinylated NAD^+), activated (damaged) DNA, and PARP buffer (in a 1:1:8 ratio) was introduced into each well using a multichannel pipette. The mixtures were incubated for 60 min at room temperature followed by four washes using 0.1% Triton X-100 in PBS. Each well was then incubated for a further 60 min at room temperature in the presence of the supplied Strep-HPR conjugate (diluted 500-fold) followed by four washes using 0.1% Triton X-100 in PBS. Finally, TACS-Sapphire™ was introduced into each well and the colorimetric reaction was allowed to develop over 15 min at room temperature in the dark; the reaction was terminated by adding 0.2 M HCl. Absorbance measurements were performed at 450 nm using a Tecan Infinite M200 Pro microplate reader and were normalized to the positive and negative control values. The mean absorbance measurements were plotted against the corresponding log concentrations of each compound under investigation and a four-parameter logistic model was fitted to the resulting curves using the GraphPad Prism 6.0 software allowing for calculation of the IC_{50}. The reported IC_{50} values for each compound were based on three experiments.

Cell culture. G7 and T98G human glioblastoma cell lines were cultured in Dulbecco's Modified Eagle Medium (DMEM) supplemented with 10% fetal calf serum (FCS), 2 mM L-glutamine and 1 mM sodium pyruvate and Minimum Essential Media (MEM) supplemented with 10% FCS and 2 mM L-glutamine respectively. All cellular incubations were performed at 37 °C and 5% CO_2 unless stated otherwise.

Cellular IC_{50}. Cells were seeded onto glass coverslips (19 mm dia.) in 12-well plates at concentrations of 8×10^4 (G7) or 5×10^4 (T98G) cells per well and were incubated for 48 h. The cells were then incubated for 60 min in cell media containing increasing concentrations of compounds **1** or **5**. The compounds were dissolved in DMSO followed by serial dilution using PBS to generate the necessary stock solutions; the final dilutions used to attain the desired assay concentrations were performed using cell media and the final concentration of DMSO in each case was <1%. Next, the coverslips were incubated in 20 mM H_2O_2 in PBS in the dark, at room temperature for 10 min. A negative control containing media alone minus H_2O_2 treatment, and a positive control containing media alone plus H_2O_2 treatment were also used. The cells were washed with PBS and fixed with ice cold 4% formaldehyde in PBS for 15 min. Following fixation the cells were washed with PBS, permeabilized with 0.3% Triton X-100 in PBS for 10 min at room temperature, and then washed three more times with PBS. The fixed cells were then incubated in 2% bovine serum albumin (BSA) in PBS for 30 min at room temperature. Primary antibody staining was performed using 1:200 anti-PADPR antibody (mouse antibody; ab14459; 10H; Abcam) in KB buffer (10 mM Tris pH 7.5, 150 mM NaCl, 0.1% BSA) by incubating the coverslips on parafilm at room temperature for 60 min. The coverslips were washed once with PBS and twice with KB buffer and secondary staining was performed by using 1:500 anti-mouse antibody (goat anti-mouse antibody; Alexa Fluor 488; A11029; Life Technologies) in KB buffer by incubating the fixed cells at room temperature in the dark for 60 min. The coverslips were then washed three times with KB buffer and mounted onto glass slides using VectaShield® mounting medium. Immunofluorescence imaging was performed within 48 h of staining using a Zeiss LSM 710 confocal microscope. The following imaging parameters were used: 40 × magnification (oil); resolution = 512 × 512; tiling = 3 × 3; Z-stacking = 3–4 sections, image

depth = 12 bit. PARP activity was expressed as a ratio of poly(ADP-ribose) positive nuclei to the total number of nuclei; nuclei counted per well >120. Mean PARP activity was normalized to the positive and negative control values and plotted against the corresponding log concentrations of each compound under investigation. A four-parameter logistic model was fitted to the resulting curves using the GraphPad Prism 6.0 software allowing for calculation of the IC_{50}. The reported IC_{50} values for each compound were based on two experiments.

Plasma stability. Blood was harvested from female black-6 mice and to 0.5–1.0 mL of blood was added 75 μL of 0.5 M EDTA in dH_2O. The blood was centrifuged at 5000 g for 5 min at room temperature and the plasma supernatant was isolated. To 50 μL of mouse plasma supernatant was added 10 μL of 250 μM **1** or **5** stock solution made in DMSO and dH_2O such that the final assay concentration of DMSO was <1%. A negative control containing 50 μL of dH_2O and 10 μL of 250 μM test compound minus plasma proteins was also used. The mixtures were incubated at room temperature for either 0 or 20 h, followed by addition of 200 μL of ice cold MeOH to precipitate the plasma proteins which were then isolated through centrifugation at 2000 g for 5 min at room temperature. The supernatant (100 μL) was diluted with 300 μL of a 50:50 MeCN: dH_2O solution and 10 μL of 250 μM internal standard (compound **13**) was added. The resulting solution was passed through a 0.22 μm filter and analyzed using liquid chromatography-mass spectroscopy, LC-MS (Shimadzu LC-2010AHT, LCMS-2010EV). LC was performed on 20 μL sample injections using a Kinetex 5 μm XB-C18 100Å (50 × 4.60 mm) column and the following mobile phase conditions: 0.0–10.0 min 30:70 to 60:40 A:B, 10.0–12.0 min 60:40 to 30:70 A:B, 12.0–14.0 min 30:70 A:B where A = MeCN and B = 0.1% formic acid in dH_2O; flow rate 1.2 mL/min. The internal standard and parent compounds were detected using MS under the following conditions: positive ionisation; detector 1.50 kV; SIM m/z 551 (internal

standard: compound **13**; MH^+) and 597 (compound **5**; MH^+). Quantification was performed using the LabSolutions LCMS (Shimadzu Corporation) software by calculating the mean ratio of the area under the peak of the test compound to the internal standard. This ratio was then expressed as the percentage of parent compound (%parent) remaining relative to the negative control and a bar graph was plotted using the GraphPad Prism 6 software; error bars represent %parent remaining + standard deviation. The reported values for each compound were based on three experiments.

Intrinsic Clearance (Cl_{int}). Aliquots (100 μL) of Gibco® pooled human liver microsomes from 50 donors (20 mg/mL) were diluted with 100 mM KH_2PO_4 buffer (pH 7.4) such that the microsomal concentration was 10 mg/mL. The diluted microsomal enzyme stock (10 μL) was added to 160 μL of 100 mM KH_2PO_4 buffer (pH 7.4) followed by 10 μL of 60 μM **1** or **5** in a mixture of DMSO and 100 mM KH_2PO_4 buffer (pH 7.4) such that the final assay concentration of DMSO was ≤1%. The solutions were warmed to 37 °C for 10 min followed by addition of 20 μL of 13 mM NADPH stock in 100 mM KH_2PO_4 buffer (pH 7.4). A negative control was used which contained 10 μL of the diluted microsomal enzyme stock, 10 μL of 60 μM test compound solution and 180 μL of 100 mM KH_2PO_4 buffer (pH 7.4) minus NADPH. Incubations were terminated 0, 5, 15, 30 and 45 min after NADPH addition by introducing 200 μL of MeCN which precipitated the microsomal enzymes. The suspensions were centrifuged at 1000 g for 5 min at room temperature and 350 μL of the supernatant was removed from each sample and diluted with 200 μL of MeCN followed by the addition of 10 μL of 60 μM internal standard (compound **13** for compound **5** or papaverine for compound **1**). The resulting solutions were passed through a 0.22 μm filter and were analyzed using LC-MS (Shimadzu LC-2010AHT, LCMS-2010EV). LC was performed on 40 μL sample injections using a Kinetex 5 μm XB-C18

100Å (50 × 4.60 mm) column. The mobile phase conditions were dependant on the test compound: i) **5** 0.0–10.0 min 30:70 to 60:40 A:B, 10.0–10.5 min 60:40 to 90:10 A:B, 10.5–12.0 min 90:10 A:B, 12.0–12.5 min 90:10 to 30:70 A:B, 12.5–15.0 min 30:70 A:B; and ii) **1** 0.0–10.0 min 20:80 to 55:45 A:B, 10.0–12.0 min 55:45 to 20:80 A:B, 12.0–14.0 min 20:80 A:B where A = MeCN and B = 0.1% formic acid in dH_2O; flow rate 1.2 mL/min. The internal standards and parent compounds were detected using MS under the following conditions: positive ionisation; detector 1.50 kV; SIM m/z 551 (internal standard: compound **13**; MH^+), 597 (compound **5**; MH^+), 340 (internal standard: papaverine; MH^+), 435 (compound **1**; MH^+). Quantification was performed using the LabSolutions LCMS (Shimadzu Corporation) software by calculating the ratio of the area under the peak of the test article to the internal standard. This ratio was then expressed as the ln % of parent remaining relative to the 0 min incubation timepoint. Ln % of parent remaining over time plots were generated using the GraphPad Prism 6 software and linear regression models were used to calculate the Cl_{int} of the test compound using the following equations:[27]

i) $k = -\text{gradient}$

ii) $t_{1/2}$ (min) = ln(2)/k

iii) Vd (μL/mg) = volume of incubation (μL) ÷ protein in incubation (mg)

iv) Cl_{int} (μL/min/mg of protein) = (Vd × ln(2)) ÷ $t_{1/2}$

where k = elimination rate constant, $t_{1/2}$ = half-life, and Vd = volume of distribution. The reported Cl_{int} values for each compound were based on two experiments.

Radiochemistry. A 2.00 mL v-vial was half-filled with 3 mm borsilicate glass beads and to that was added 100 μL of 0.492 M $(NH_4)_2SO_4$ solution in dH_2O and 100 μL of 1.68 mM solution of

precursor **13** in glacial acetic acid. The mixture was vortexed and then 35.5–175.0 MBq of [^{123}I]-NaI in 50.0 mM NaOH was added; the edges of the v-vial were rinsed with 150 μL of EtOH:dH_2O (1:2). Solvents were removed by passing a constant stream of argon over the solution at 150 °C and aliquots of anhydrous MeCN (3 × 500 μL) were added to facilitate azeotropic drying (approx. 30 min). The argon supply was removed and the sealed v-vial was heated to 210 °C. Once at the correct temperature, 8 mL of air was injected and the reaction was heated for a further 30 min. The contents of the v-vial were allowed to cool to room temperature and the organic components were dissolved in 300 μL of MeCN followed by the addition of 150 μL of MeCN:dH_2O (3:7). The crude [^{123}I]-**5** reaction mixture was loaded onto a Phenomenex Synergi 4 μm Hydro-RP 80Å (150 × 10.00 mm) column. Purification was achieved using a Dionex Ultimate 3000 HPLC system and the following mobile phase conditions: 0.0–30.0 min 30:70 A:B to 55:45 A:B where A = MeCN and B = dH_2O; flow rate 3.0 mL/min. Detection was achieved using a Knauer Advanced Scientific Instruments Smartline UV Detector 2500 (254 nm) and a photomultiplier tube connected to a Lab Logic Flow-Count radiodetector. The radiolabeled product was collected at approximately 27.0 min and concentrated *in vacuo* in an evaporator flask. The flask was rinsed with MeCN (3 × 300 μL) to extract the radiolabeled compound and the solution was transferred to a 2.00 mL v-vial; the solvent was removed by passing a constant stream of argon over the solution at 100 °C (approx. 15 min). The radiotracer was then reconstituted in up to 900 μL of a 10% EtOH in 0.9% saline solution. Since the amount of radiolabeled product that was produced fell below the sensitivity threshold of the UV detector (<1.68 × 10^{-4} μmol), specific activity (Ci/μmol) was calculated using the lowest detectable amount of non-labelled **5** established from a calibration plot of a range of concentrations (0.001–1.000 mg/mL). The identity of the radiolabeled product was confirmed by performing quality

control analysis of a sample of the formulated radiotracer using a Dionex Ultimate 3000 HPLC system and a Phenomenex Synergi 4 μm Hydro-RP 80Å (150 × 4.60 mm) column. The same mobile phase conditions were used as described above for the HPLC purification step. Radiodetection was achieved using a Berthold Technologies Flow Star LB513 detector. All HPLC analyses were performed using the Chromeleon 6.8 Chromatography software.

Mouse Glioma Model. Female 7–11 week old CD1 nude mice had 5×10^6 U87MG-Luc2 cells injected subcutaneously into the right flank. The U87MG-Luc2 cells were originally derived from a glioblastoma (stage IV) in a 44 year old male Caucasian patient; the cell line was purchased commercially from ATCC. The animal subcutaneous xenografts were measured and monitored visually every three days. Tumor bearing animals were used for in vivo studies 21–30 days post-implantation.

***Ex vivo* Biodistribution.** Subcutaneous tumor bearing mice received bolus tail vein injections of 0.8–1.1 MBq [^{123}I]-**5** in 0.15–0.25 mL 10% EtOH in 0.9% saline. The animals were sacrificed by CO_2 asphyxiation either 30 min (n=3), 60 min (n = 4) or 120 min (n=4) following tracer injection. The following tissue and material were harvested and transferred to pre-weighed 1.5 mL Eppendorf vials containing 0.5 mL of fixative (4% formaldehyde in PBS) immediately after sacrifice: i) blood, ii) spleen, iii) stomach matter, iv) stomach tissue, v) small bowel matter, vi) small bowel tissue, vii) caecum matter, viii) large bowel tissue, ix) solid faeces, x) pancreas, xi) liver (left lobe), xii) kidney (left), xiii) heart, xiv) lung (left lobe), xv) muscle (left femur), xvi) femur (left), xvii) brain, and xviii) tumor. Each vial was weighed and gamma counted using a Cobra II Auto-Gamma® counter using the following parameters: count time = 1 min; KeV range = 136–215; output = counts per min (CPM). A positive control was used containing 0.5 mL of fixative and 10 μL of the [^{123}I]-**5** stock solution used to dose the animal. Background counts were

defined using a negative control containing 0.5 mL of fixative. The background signal was subtracted and the CPM were normalized to the weight of each tissue or matter sample. The CPM of each positive control were then used to calculate the theoretical maximum CPM of each injected tracer volume and this was in turn used to calculate the percentage injected dose per gram of tissue or matter (%ID/g). Calculations were performed using the Microsoft Excel 2010 software. The mean %ID/g acquired for each tissue or material was plotted on a bar chart using the GraphPad Prism 6.0 software; error bars represent the %ID/g + SD.

Ex vivo **Biodistribution pre-blockade.** Subcutaneous tumor bearing mice received an intraperitoneal injection of either vehicle (13.5% DMSO and 10% 2-hydroxy-β-cyclodextrin in dH_2O) (n = 3) or 50 mg/kg of compound **1** in vehicle 20 min prior to intravenous tail vein injection of 0.8–1.1 MBq [^{123}I]-**5** in 0.18–0.25 mL 10% EtOH in 0.9% saline. The animals were sacrificed by CO_2 asphyxiation 60 min after tracer injection, and tumor and muscle tissues were immediately harvested and transferred to pre-weighed 1.5 mL Eppendorf vials containing 0.5 mL of fixative (4% formaldehyde in PBS). Each vial was gamma counted and the %ID/g values were calculated as described earlier. The data were plotted on a bar chart as the ratio of %ID/g of tumor to muscle tissue using the GraphPad Prism 6.0 software; error bars represent the %ID/g + SD.

Immunohistochemistry. Tumor and muscle tissues were immersion fixed in 4% formaldehyde for 48 h. The fixed tissues were embeded in paraffin blocks and 4 μm sections were cut. Paraffin was removed by incubating the tissue sections in xylene (2 × 5 min) followed a 5 step rehydration using 100% EtOH (1 min and 5 min), 70% EtOH (2 × 5 min) and water (5 min). Immunohistochemistry was performed using the Dako EnVision™ kits. Briefly, heat induced antigen retrieval using Dako Cytomation Target Retrieval Solution (pH 6.0) was followed by an

incubation in 3% H_2O_2 in MeOH (20 min), and then 5% BSA and 5% goat serum in PBS (20 min) to block peroxidase activity and minimize non-specific binding respectively. Between each step the tissue sections were washed in 0.1% Tween® 20 in TBS (2 × 5 min). The tissue sections were incubated overnight at 4–8 °C in 1:100 anti-PARP-1 antibody (mouse anti-human and mouse antibody; sc-8007; Santa Cruz). Following this, the tissue was washed with 0.1% Tween® 20 in TBS (2 × 5 min) and a secondary one hour incubation at room temperature was performed using Dako horseradish-peroxidase labeled anti-mouse polymer. The sections were once again washed using 0.1% Tween® 20 in TBS (2 × 5 min) and the presence of antibody was detected using a 3,3'-diaminobenzidine chromagen solution diluted in Dako DAB^+ substrate buffer. Haematoxylin and eosin staining was performed using a Leica ST5020 multistainer. Histology images were acquired using a Zeiss AX10 brightfield microscope at ×4 magnification and contrast was corrected manually using the ImageJ 1.47v software.

ANCILLARY INFORMATION

Supporting Information: Synthesis of the penultimate compound **6**; ^1H and ^{13}C-NMR spectra for all new compounds; cell-free and cellular IC_{50} curves; plasma stability graph for compound **5**; metabolic stability graphs for **1** and **5**; radiochemistry HPLC chromatograms.

Corresponding Author Information:

*Telephone: +44 (0)141 301 7821; Fax: +44 (0)141 301 7821

Email: sally.pimlott@glasgow.ac.uk

Address: PET Radiopharmaceutical Production Unit, West of Scotland PET Centre, Gartnavel General Hospital, 1053 Great Western Road, Glasgow, G12 0YN, UK.

Notes:

The authors declare no competing financial interest.

Acknowledgment:

The authors would like to acknowledge Dr Shafiq Ahmed for providing guidance concerning the cellular IC_{50} assays, and Dr Lesley Gilmour and Sandeep Chahal for their input in setting up the necessary small animal xenograft models. The authors would also like to gratefully acknowledge financial support from the University of Glasgow (studentship FZ), EPSRC (EP/J500434) and the Cancer Research UK Glasgow Centre Development Fund.

Abbreviations:

CHI, chromatographic hydrophobicity index; CHIN, non-ionized chromatographic hydrophobicity index; CI, confidence interval; Cl_{int}, intrinsic clearance; CPM, counts per minute; CT, computed tomography; dH_2O, distilled water; DSB, double-stranded DNA breaks; DMEM, Dulbecco's modified eagle medium; EU, Europe; FCS, fetal calf serum; GBM, glioblastoma; HBC, hydrogen-bond donor count; ID/g, injected dose per gram of material; IPA, iso-propyl alcohol; Log K, logarithm of retention factor; MBq, megabequerel; MEM, minimum essential media; PADPR, poly(ADP-ribose); PARP-1, poly(ADP-ribose) polymerase-1; PARPi, PARP-1 inhibitors; SD, standard deviation; SSB, single-stranded DNA breaks; Strep-HPR, streptavidin-horseradish peroxidase; TBS, tris-buffered saline; $t_{1/2}$, half-life; US, United States of America; Vd, volume of distribution.

REFERENCES:

1. Weaver, A. N.; Yang, S.Y. Beyond DNA repair: additional functions of PARP-1 in cancer. Front. Oncol. **2013**, 3, 1–11.

2. Ferraris, D. V. Evolution of poly(ADP-ribose) polymerase-1 (PARP-1) inhibitors. From concepts to clinic. J. Med. Chem. **2010**, 53, 4561–4584.

3. Rouleau, M.; Patel, A.; Hendzel, M. J.; Kaufmann, S. H.; Poirier, G. G. PARP inhibition: PARP1 and beyond. Nat. Rev. Cancer **2010**, 10, 293–301.

4. Deeks, E. D. Olaparib: first global approval. Drugs **2015**, 75, 231–240.

5. Plummer, R.; Jones, C.; Middleton, M.; Wilson, R.; Evans, J.; Olsen, A.; Curtin, N.; Boddy, A.; McHugh, P.; Newell, D.; Harris, A.; Johnson, P.; Steinfeldt, H.; Dewji, R.; Wang, D.; Robson, L.; Calvert, H. Phase I study of the poly(ADP-ribose) polymerase inhibitor, AG014699, in combination with temozolomide in patients with advanced solid tumors. Clin. Cancer Res. **2008**, 14, 7917–7923.

6. Isakoff, S. J.; Overmoyer, B.; Tung, N. M.; Gelman, R. S.; Giranda, V. L.; Bernhard, K. M.; Habin, K. R.; Ellisen, L. W.; Winer, E. P.; Goss, P. E. A phase II trial of the PARP inhibitor veliparib (ABT888) and temozolomide for metastatic breast cancer. J. Clin. Oncol. **2010**, 28, suppl; abstr 1019.

7. Khan, O. A.; Gore, M.; Lorigan, P.; Stone, J.; Greystoke, A.; Burke, W.; Carmichael, J.; Watson, A. J.; McGown, G.; Thorncroft, M.; Margison, G. P.; Califano, R.; Larkin, J.; Wellman, S.; Middleton, M. R. A phase I study of the safety and tolerability of olaparib (AZD2281, KU0059436) and dacarbazine in patients with advanced solid tumours. Br. J. Cancer **2011**, 104, 750–755.

8. Rajan, A.; Carter, C. A.; Kelly, R. J.; Gutierrea, M.; Kummar, S.; Szabo, E.; Yancey, M. A.; Ji, J.; Mannargudi, B.; Woo, S.; Spencer, S.; Figg, W. D.; Giaccone, G. A phase I combination study of olaparib with cisplatin and gemcitabine in adults with solid tumors. Clin. Cancer Res. **2012**, 18, 2344–2351.

9. Samol, J.; Ranson, M.; Scott, E.; Macpherson, E.; Carmichael, J.; Thomas, A.; Cassidy, J. Safety and tolerability of the poly(ADP-ribose) polymerase (PARP) inhibitor, olaparib (AZD2281) in combination with topotecan for the treatment of patients with advanced solid tumors: a phase I study. Invest. New Drugs **2012**, 30, 1493–1500.

10. Dent, R. A.; Lindeman, G. J.; Clemons, M.; Wildiers, M.; Chan, A.; McCarthy, N. J.; Singer, C. F.; Lowe, E. S.; Watkins, C. L.; Carmichael, J. Phase I trial of the oral PARP inhibitor olaparib in combination with paclitaxel for first- or second-line treatment of patients with metastatic triple-negative breast cancer. Breast Cancer Res. **2013**, 15, R88.

11. Galia, A.; Calogero, A. E.; Conderelli, R. A.; Fraggetta, F.; Corte, C.; Ridolfo, F.; Bosco, P.; Castiglione, R.; Salemi, M. PARP-1 protein expression in glioblastoma multiforme. Eur. J. Histochem. **2012**, 56, 45–48.

12. Pirotte, B. J.; Levivier, M.; Goldman, S.; Massager, N.; Wikler, D.; Dewitte, O.; Bruneau, M.; Rorive, S.; David, P.; Brotchi, J. Positron emission tomography-guided volumetric resection

of supratentorial high-grade gliomas: a survival analysis in 66 consecutive patients. Neurosurgery **2009**, 63, 471–481.

13. Reiner, T.; Lacy, J.; Keliher, E. J,; Yang, K. S.; Ullal, A.; Kohler, R. H.; Vinegoni, C.; Weissleder, R. Imaging therapeutic PARP inhibition in vivo through bioorthogonally developed imaging agents. Neoplasia **2012**, 14, 169–177.

14. Zhou, D.; Chu, W.; Xu, J.; Jones, L. A.; Peng, X.; Li, S.; Chen, D. L.; Mach, R. H. Synthesis, [^{18}F] radiolabelling, and evaluation of poly (ADP-ribose) polymerase-1 (PARP-1) inhibitors for in vivo imaging of PARP-1 using positron emission tomography. Bioorg. Med. Chem. **2014**, 22, 1700–1707.

15. Carlucci, G.; Carney, B.; Brand, C.; Kossatz, S.; Irwin, C. P.; Carlin, S. D.; Keliher, E. J.; Weber, W.; Reiner, T. Dual-modality optical/PET imaging of PARP-1 in glioblastoma. Mol. Imaging Biol. [Online early access]. DOI: 10.1007/s11307-015-0858-0. Published Online: April 17, 2015.

16. Rahmim, A.; Zaidi, H. PET versus SPECT: strengths, limitations and challenges. Nucl. Med. Commun. **2008**, 29, 193–207.

17. Ritt, P.; Kuwert, T. SPECT/CT technology. Clin. Transl. Imaging **2014**, 2, 445–457.

18. European Association of Nuclear Medicine. Status of nuclear medicine in Europe. **2010**. Available from: http://www.kfnm.dk/div/Results_EANM_Survey_2010.pdf (accessed 23 June 2015).

19. Cockroft, X.; Dillon, K. J.; Dixon, L.; Drzewiecki, J.; Kerrigan, F.; Loh, V. M.; Martin, N. M. B.; Menear, K. A.; Smith, G. C. M. Phthalazinones 2: optimisation and synthesis of novel

potent inhibitors of poly(ADP-ribose) polymerase. Bioorg. Med. Chem. Lett. **2006,** 16, 1040–1044.

20. Menear, K. A.; Adcock, C.; Boulter, R.; Cockroft, X.; Copsey, L.; Cranston, A.; Dillon, K. J.; Drzewiecki, J.; Garman, S.; Gomez, S.; Javaid, H.; Kerrigan, F.; Knights, C.; Lau, A.; Loh, V. M.; Matthews, I. T. W.; Moore, S.; O'Connor, M. J.; Smith, G. C. M.; Martin, N. M. B. 4-[3-(4-cyclopropanecarbonylpiperazine-1-carbonyl)-4-fluorobenzyl]-2H-phthalazin-1-one: a novel bioavailable inhibitor of poly(ADP-ribose) polymerase-1. J. Med. Chem. **2008**, 51, 6581–6591.

21. Arnott, J. A.; Planey, S. L. The influence of lipophilicity in drug discovery and design. Expert Opin. Drug Discovery **2012**, 7, 863–875.

22. Jacobson, O.; Chen, X. Interrogating tumor metabolism and tumor microenvironments using molecular positron emission tomography imaging. Theranostic approaches to improve therapeutics. Pharmacol. Rev. **2013**, 65, 1214–1256.

23. Abbott, N. J.; Patabendige, A. A. K.; Dolman, D. E. M.; Yusof, S. R.; Begley, D. J. Structure and function of the blood-brain barrier. Neurobiol. Dis. **2010**, 37, 13–25.

24. Stehe, G.; Sinn, H.; Wunder, A.; Schrenk, H. H.; Stewart, J. C. M.; Hartung, G.; Maier-Borst, W.; Heene, D. L. Plasma protein (albumin) catabolism by the tumor itself – implications for tumor metabolism and the genesis of cachexia. Crit. Rev. Oncol. Hematol. **1997**, 26, 77–100.

25. Kremer, P.; Fardanesh, M.; Ding, R.; Pritsch, M.; Zoubaa, S.; Frei, E. Intraoperative fluorescence staining of malignant brain tumors using 5-aminofluorescein-labeled albumin. Neurosurgery **2009**, 64, suppl: ons 53–60.

26. Leppäla, J.; Kallio, M.; Nikula, T.; Nikkinen, P.; Liewendahl, K.; Jääskläinen, J.; Savolainen, S.; Gylling, H.; Hiltunen, J.; Callaway, J.; Khal, S.; Färkkilä, M. Accumulation of ^{99m}Tc-low-density lipoprotein in human malignant glioma. Br. J. Cancer **1995**, 71, 383–387.

27. Obach, R. S. Prediction of human clearance of twenty-nine drugs from hepatic microsomal intrinsic clearance data: an examination of in vitro half-life approach and nonspecific binding to microsomes. Drug. Metab. Dispos. **1999**, 27, 1350–1359.

28. Scott, M. T.; Sinsheimer, J. E. In vitro dehalogenation of para- substituted aromatic halides in rat liver preparations. J. Pharm. Sci. **1984,** 73, 1101–1104.

29. Gagnon, A.; Amad, M. H.; Bonneau, P. R.; Coulombe, R.; DeRoy, P. L.; Doyon, L.; Duan, J.; Garneau, M.; Guse, I.; Jakalian, A.; Jolicoeur, E.; Landry, S.; Malenfant, E.; Simoneau, B.; Yoakim, C. Thiotetrazole alkynylacetanilides as potent bioavailable non-nucleoside inhibitors of the HIV-1 wild type and K103N/Y181C double mutant reverse transcriptases. Bioorg. Med. Chem. Lett. **2007**, 17, 4437–4441.

30. Pimlott, S. L.; Stevenson, L.; Wyper, D. J.; Sutherland, A. Rapid and efficient radiosynthesis of [^{123}I]I-PK11195, a single photon emission computed tomography tracer for peripheral benzodiazepine receptors. Nucl. Med. Biol. **2008**, 35, 537–542.

31. Gildersleeve, D. L.; Van Dort, M. E.; Johnson, J. W.; Sherman, P. S.; Wieland, D. M. Synthesis and evaluation of [^{123}I]-iodo-PK11195 for mapping peripheral-type benzodiazepine receptors (ω_3) in heart. Nucl. Med. Biol. **1996**, 23, 23–28.

32. Mangner, T. J.; Wu, J.; Wieland, D. M. Solid-phase exchange radioiodination of aryl iodides. Facilitation by ammonium sulfate. J. Org. Chem. **1982**, 47, 1484–1488.

33. Ang, J. E.; Clarkson-Jones, J. A.; Swaisland, H.; Brunetto, A. T.; Lal, R.; Farnsworth, A. P.; Molife, L. R.; Kaye, S. B.; Carmichael, J.; de Bono, J. S. 405 A Mass balance study to investigate the metabolism, excretion and pharmacokinetics of [14C]-olaparib (AZD2281) in patients with advanced solid tumours refractory to standard treatments. Eur. J. Cancer Suppl. **2010**, 8, 128–129.

34. van de Waterbeemd, H.; Camenisch, G.; Folkers, G.; Chretien, J. R.; Raevsky, O. A. Estimation of blood-brain barrier crossing of drugs using molecular size, shape, and H-bonding descriptors. J. Drug Targeting **1998**, 6, 151–165.

35. Tavares, A. A. S.; Lewsey, J.; Dewar, D.; Pimlott, S. L. Radiotracer properties determined by high performance liquid chromatography: a potential tool for brain radiotracer discovery. Nucl. Med. Biol. **2012**, 39, 127–135.

36. Chalmers, A. J.; Jackson, A.; Swaisland, H.; Stewart, W.; Halford, S. E. R.; Molife, L. R.; Hargrave, D. R.; McCormick, A. Results of stage 1 of the operatic trial: a phase I study of olaparib in combination with temozolomide in patients with relapsed glioblastoma. J. Clin. Oncol. **2014**, 32, suppl; abstr 2025.

37. Moussa, I. A.; Banister, S. D.; Beinat, C.; Giboureau, N.; Reynolds, A. J.; Kassiou, M. Design, synthesis and structure-affinity relationships of regioisomeric N-benzyl alkyl ether piperazine derivatives as σ-1 receptor ligands. J. Med. Chem. **2010**, 53, 6228–6239.

38. Valkó, K.; Bevan, C.; Reynolds, D. Chromatographic hydrophobicity index by fast-gradient RP-HPLC: a high-throughput alternative to log P/log D. Anal. Chem. **1997**, 69, 2022–2029.

39. Valkó, K. Application of high-performance liquid chromatography based measurements of lipophilicity to model biological distribution. J. Chromatogr. A. **2004**, 1037, 299–310.

40. Valkó, K.; Nunhuck, S.; Bevan, C.; Abraham, M.; Reynolds, D. Fast gradient HPLC method to determine compounds binding to human serum albumin. Relationships with octanol/water and immobilized artificial membrane lipophilicity. J. Pharm. Sci. **2003**, 92, 2236–2248.

Tables, Figures and Schemes.

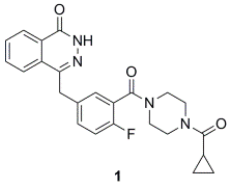

Figure 1. The clinical PARP-1 inhibitor olaparib.

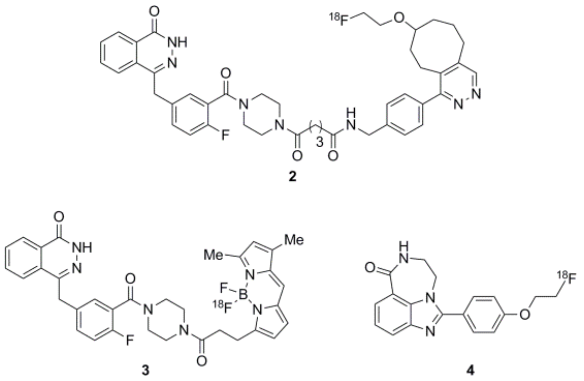

Figure 2. PARP-1 PET imaging tracers currently in development.[13–15]

Table 1. Approach used to access **1** and analogs **5** and **7–12**, from the penultimate compound **6**, as well as the cell-free PARP-1 inhibitory and physiochemical properties of these compounds.

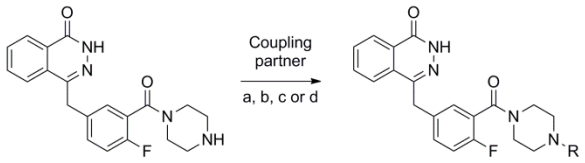

6 **1, 5, 7–12**

Coupling partner	Coupling conditions	R	Yield (%)	Cell-free IC_{50} (95% CI), nM[a]	Log P_{oct}[b]	%PPB[c]
	a	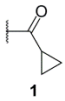 **1**	51	11.9 (10.5–13.6)	1.95	75.9
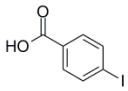	b	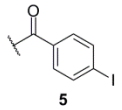 **5**	34	3.3 (2.6–4.2)	3.00	96.2
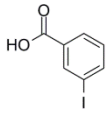	b	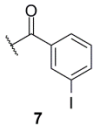 **7**	45	3.9 (3.4–4.4)	2.97	96.1
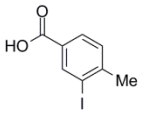	c	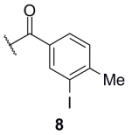 **8**	48	16.9 (12.5–22.9)	3.23	97.6
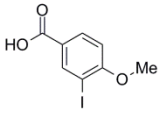	b	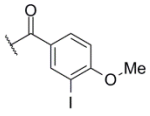 **9**	26	17.6 (14.3–21.7)	2.95	96.5
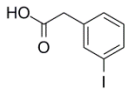	b	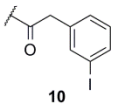 **10**	40	5.8 (4.9–6.8)	3.13	97.5
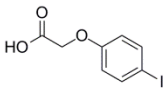	b	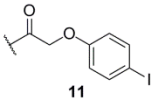 **11**	32	3.0 (2.5–3.6)	3.25	98.1
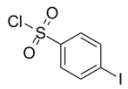	d	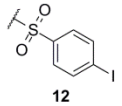 **12**	52	22.6 (18.5–27.6)	>3.25[d]	98.4

Reagents and conditions: (a) HBTU, Et_3N, DMF, rt, 72 h; (b) HBTU, Et_3N, DMF, rt, 48 h; (c) HBTU, Et_3N, DMF, 40 °C, 22 h; (d) Et_3N, CH_2Cl_2, rt, 6 h.

[a]Cell-free IC_{50} values are based on three experiments. [b]Lipophilicity (log P_{oct}) was determined using a C-18 reverse phase HPLC column. [c]Percentage plasma protein binding (%PPB) was determined using a human serum albumin coated HPLC column. [d]The exact log P_{oct} could not be calculated as the value exceeded the assay limit.

Table 2. Cellular PARP-1 inhibitory, and mouse plasma and metabolic stability properties of compounds **1** and **5**.

Compound	Cellular IC_{50} (95% CI), nM[a] G7	T98G	Plasma stability[b]	Cl_{int} (± SD), µL/min/mg[c]
1	1.6 (1.4–1.8)	1.6 (1.4–1.8)	-	29 (± 8)
5	7.0 (6.3–7.9)	7.4 (6.4–8.5)	98 ± 9%	85 (± 4)

[a]Cellular IC_{50} values obtained using primary G7 and established T98G human glioblastoma cell lines are based on two experiments. [b]The mean percentage of parent compound remaining after a 20 h incubation in mouse plasma (± SD of three experiments) was ascertained for compound **5**. [c]Intrinsic clearance (Cl_{int}) values are the mean ± SD of two experiments.

Table 3. Optimization of the solid state halogen exchange radioiodination methodology using brominated precursor **13**.

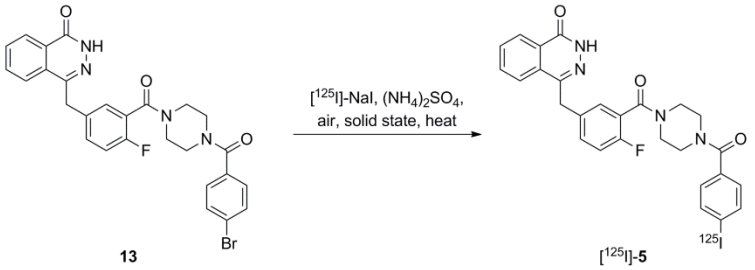

Entry	Air injection	Temperature (°C)	Reaction time (min)	^{125}I incorporation (%)[a]
1	Yes	150	20	38
2	Yes	180	30	78
3	Yes	210	30	90
4	No	210	30	66

[a]Calculated from the radio-HPLC trace following a single reaction.

Scheme 1. Optimized radioiodination approach used to generate [^{123}I]-**5**.

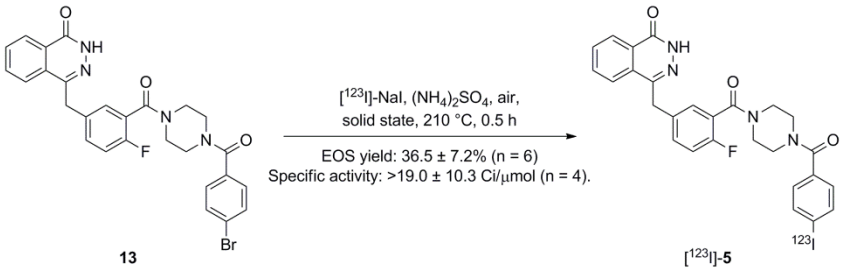

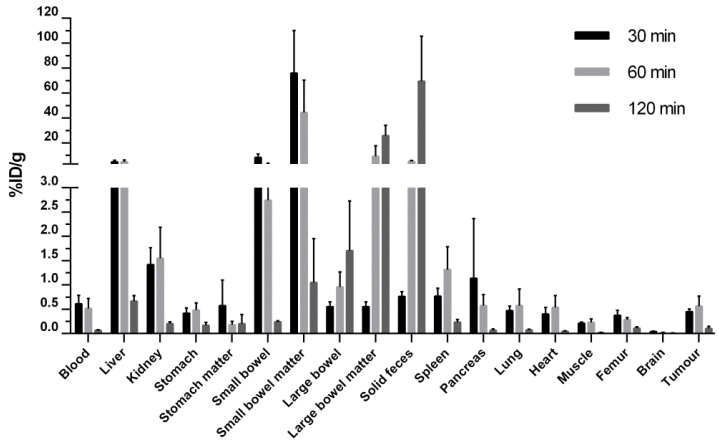

Figure 3. *Ex vivo* biodistribution of [^{123}I]-**5** in subcutaneous human glioblastoma bearing nude mice 30 min (n = 3), 60 min (n = 4) and 120 min (n = 4) after tracer injection. Error bars represent the mean percentage of injected dose per gram of tissue or material (% ID/g) + SD.

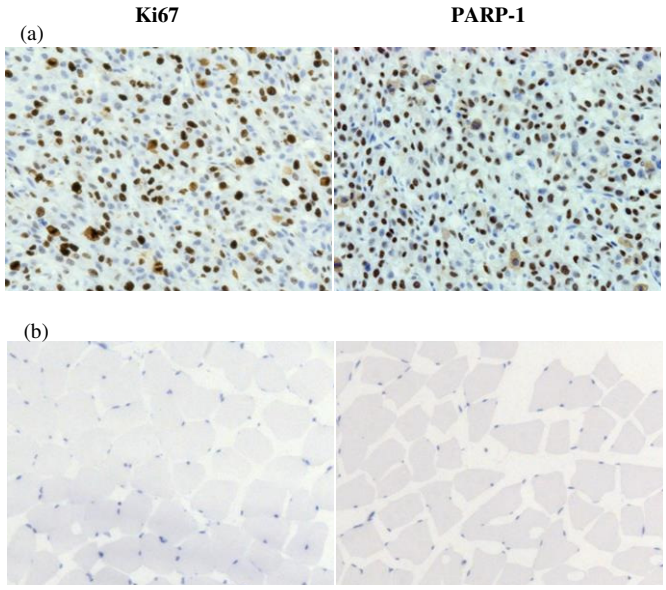

Figure 4. Representative immunohistochemistry images of a U87MG-Luc2 subcutaneous tumor (a) and muscle tissue (b) stained for the cell proliferation marker Ki67 and PARP-1. The tissues were counterstained with hematoxylin. Brown staining signifies presence of marker and dark blue staining shows cellular nuclei.

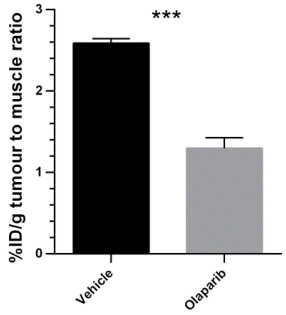

Figure 5. Ratio of percentage of injected dose per gram (%ID/g) of tumor to muscle of [^{123}I]-**5** 60 min after injection in subcutaneous human glioblastoma bearing nude mice pre-treated with either vehicle (n = 3) or 50 mg/kg compound **1** (n = 3). Error bars represent the mean + SD. Unpaired t test: P = 0.001.

Table of Contents graphic.

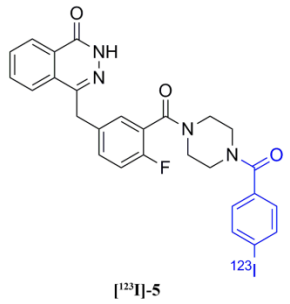

[^{123}I]-5